IEEE Access
Multidisciplinary | Rapid Review | Open Access Journal

SPECIAL SECTION ON EVOLVING TECHNOLOGIES IN ENERGY STORAGE SYSTEMS FOR ENERGY SYSTEMS APPLICATIONS

Received August 12, 2020, accepted August 28, 2020, date of publication September 28, 2020, date of current version October 9, 2020.

Digital Object Identifier 10.1109/ACCESS.2020.3027519

Upper Bound Performance of Shipboard Power and Energy Systems for Early-Stage Design

GREGORY L. SINSLEY, (Member, IEEE), DANIEL F. OPILA, (Member, IEEE), EUN S. OH, (Member, IEEE), AND JOHN D. STEVENS, (Member, IEEE)

Faculty of Electrical and Computer Engineering, United States Naval Academy, Annapolis, MD 21402, USA

Corresponding author: Gregory L. Sinsley (sinsley@usna.edu)

This work was supported by the Office of Naval Research through the Electric Ship Research and Development Consortium (ESRDC) under Contract N0001419WX00775. Distribution A, Approved for public release, distribution is unlimited. DCN# 43-5549-19.

ABSTRACT Shipboard power systems that service large-scale dynamic loads and electric propulsion can significantly improve their performance by adding controllable energy storage. These systems require power management controls that consider dynamics like generator ramp rates, along with energy storage capacity and location. In the early-stage design process, many alternative designs are considered, and each requires a unique controller. This article describes a numerical optimization technique that establishes an upper bound performance criteria without manually designing controllers for each system. The solution is a best case performance that assumes perfect future knowledge of the time-varying load. While unrealistic in real-time, this technique yields a fair comparison between competing architectures without the variability of different control methods. To demonstrate the concept, a notional multi-bus power system architecture is evaluated on a representative set of operational duties to illustrate comparisons between system attributes like energy storage power and efficiency ratings. A design trade study shows that the success rate for a baseline ship can improve from under 60% to nearly 100% by increasing generator power by 10% and energy storage capacity by 100%. These automated architecture benchmarks fit into a broader total ship optimization process, or can be used in human-driven trade studies.

INDEX TERMS Electric ship, energy storage, power flow, power system optimization, power management, pulse loads, power system control, ship design.

I. INTRODUCTION

A. MOTIVATION

Designing power systems for naval and marine vessels is increasingly challenging due to dynamic power demands from electric propulsion, positioning thrusters, cranes, sensors, weapons, and other mission loads [1], [2]. As new technologies are deployed to serve these demanding loads, the initial system design process needs better tools to study the equipment type, rating, and interconnection while considering system dynamics. Load dynamics can exceed the ramp rating of generators, so energy storage devices are often added to serve fast loads. Their specifications are critical considerations [3]–[5]. Hybrids of multiple storage technologies can handle both fast and slow power demands, and their physical location affects both performance and resiliency.

The overall ship design process must include an evaluation of the power system as a critical part of vessel capability. This multi-parameter design problem is often automated, for example in ''set-based design'' [6], and therefore requires an automated evaluation of the power system. Unfortunately, these dynamic power and energy systems require both global and local controllers [7]–[11], which must be designed in order to evaluate the system. Traditional quasi-static analysis and optimization are insufficient.

The goal of this article is to develop a method to automatically characterize system performance by determining optimal system behavior without directly designing a system controller. We seek to rigorously quantify the performance of the power system architecture independent of specific control methods.

B. LITERATURE REVIEW

Previous studies in power system architecture include optimization algorithms to design a power system or subsystems [12], [13], general architecture arrangements [14], [15], and power system resilience [16], [17].

Methods for designing the system controller include optimized power converter set points in a DC system [8], stochastic optimization [7], multi-agent systems [9], and various implementations of centralized [10] and cooperatively distributed Model Predictive Control [11]. Many of these control methods do not directly consider line flow limitations.

The associate editor coordinating the review of this manuscript and approving it for publication was Sanjeevikumar Padmanaban.

Given this variety of control methods, quantifying system performance is difficult and drives the need for automated evaluation. A quasi-static linear programming approach was used in [18]–[20] to determine what a controller should do at each instant in time, without designing the controller itself. However, controlling the system based solely on the present state as in a traditional power system will yield suboptimal solutions [21], [22]. The energy storage and generator ramping limits add system dynamics such that optimal control decisions now depend on future events. Considering future loads improves performance in many conditions [23].

C. APPROACH

This article describes an optimization method to rigorously determine the best case performance of a power system that includes time dependent dynamics without the need to design a unique controller for that system. The system controller is assumed to have full knowledge of all time varying future load power demands. This use of future demand is similar to model predictive control [10] with a very long prediction horizon, rather than the typical horizons of a few seconds. Allowing such a large prediction horizon is an optimistic assumption, but it does provide a rigorous upper bound on system performance and avoids the difficulties of selecting among thousands of possible controller designs. The results can be compared against the performance of a controller with no future knowledge [19], [20], [23].

These analysis methods are not the actual real-time controllers that go on the ship, they must merely produce a rigorous benchmark to compare candidate designs and enable quantitative system design and evaluation. Although the actual controller can never have perfect future information, it may preview load demands several seconds into the future through feedback from loads or by imposing activation delays on load requests. The quality of such a controller's preview information dictates its proximity to this upper bound benchmark [23].

The optimization problem is formulated as a multi-period extension to the standard constrained optimal power flow technique [24], [25] with the addition of energy storage capacity limits and efficiency. The results quantify performance for a specific ship configuration and mission given system constraints, and quantifies the time and location of any power or energy shortfalls. This article builds on the unconstrained analysis originally presented in [25] by solving the full multi-period optimal power flow (MP-OPF) problem with line limits and ramp rates, and quantifies trade studies on an updated system model with a much broader set of missions.

Although muti-period optimal power flow is a well known problem, it is typically studied in the context of the day-ahead planning performed by power system operators [26]. This work instead uses multi-period optimal power flow as a benchmark for an ideal controller in order to evaluate power system architectures. The metric of success is a system's ability to meet a set of dynamic loads, rather than fuel consumption [27], [28], reconfiguration in the presence of a fault [29], or other metrics.

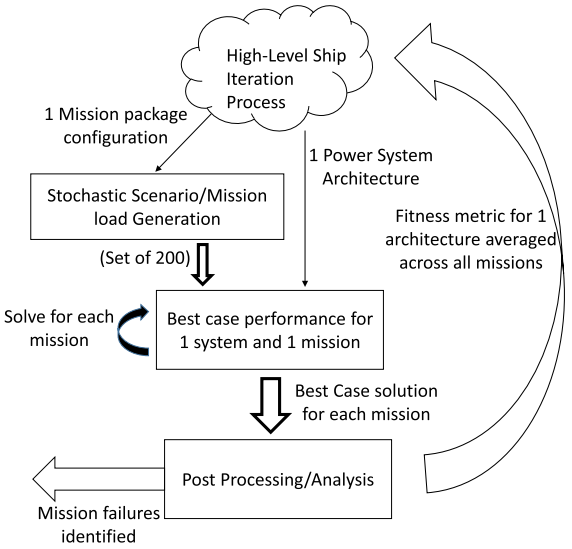

FIGURE 1. Overall design process.

D. APPLICATION

The overall ship design process consists of two optimizations: here we develop an "inner" optimization of the dynamic control for a power system to develop a fitness metric, which fits into a broader "outer" optimization that considers the overall ship design as illustrated in Fig. 1 [30], [31]. An architecture and control actions can be simultaneously optimized as in [32] for vehicle transmissions or in [27], [33] for energy storage. This has not been pursued here to keep the design process modular.

As shown in Fig. 1, for a given power system architecture and mission load package, a set of 200 mission load profiles are generated [20], [34]. Each mission represents a fixed demand profile at every bus for each time step. Load shedding is allowed but at high cost. The results in this article consider any load shedding as a mission failure because many loads will fail if curtailed. Alternatively, the load demand could be assumed to be modified in response to power shortfalls as in [35]–[37]. By using a large fixed set of missions rather than a stochastic model, the power system's fitness can be evaluated broadly, but individual mission failures and shortfalls can still be studied in detail. The results provide insight into component ratings early in the design process.

These results are then post-processed to determine an overall fitness metric for that design, which feeds into the higher-level optimization. Any mission load profiles that cannot be served with this best case performance represent a fundamental limit of the power system, and no controller exists that will serve them better. These failed missions are identified for further study to determine if they are unrealistic or truly critical.

The primary contributions of this article are as follows:

- We have developed a method to rigorously define an upper bound on the performance of a ship power

system that takes into account system static and dynamic attributes such as generator ramp limits, energy storage capacity and efficiency, and transmission line limits.
- We have performed an extensive series of trade studies using a rich set of power system load profiles in order to illustrate the ship design decisions that can be enabled via our tool.

This article is organized as follows: Section II describes a method for using optimal power flow to characterize ship power system performance. Section III presents details on a notional power system, mission load profiles, and the numerical solver. Section IV shows results for various system configurations, with applications to a ship design sequence in Section V. The results are discussed in Section VI, with conclusions in Section VII.

II. ALGORITHM FORMULATION

One goal of early stage design is to identify which missions can be accomplished with a given power system architecture, and the load shortfall for infeasible cases. This is accomplished by performing a multi-period optimal power flow problem [38]–[42]. The solution to this problem shows what an ideal controller (with perfect knowledge of future load) should do. If a demand can not be met by this optimal controller, no realizable controller could completely meet this demand. A feasible numerical solution is guaranteed by allowing unlimited load shedding p_{LS} at each bus, but at very high cost.

A. SINGLE PERIOD OPTIMAL POWER FLOW

The problem mathematically starts with a single-period general form [24], [25] for AC power

$$\min_x f(x) \tag{1}$$
$$\text{such that } g(x) = 0 \tag{2}$$
$$h(x) \leq 0 \tag{3}$$
$$x_{\min} \leq x \leq x_{\max}. \tag{4}$$

The vector of decision variables x is given as

$$x = \begin{bmatrix} V_m \\ \Theta \\ P_g \\ Q_g \end{bmatrix}. \tag{5}$$

The vectors V_m and Θ are formed from the voltage magnitude and angle, respectively, at each bus as follows

$$V_m = \left[v_{m\,1}, v_{m\,2}, \ldots, v_{m\,n_b}\right]^\top \tag{6}$$
$$\Theta = \left[\theta_1, \theta_2, \ldots, \theta_{n_b}\right]^\top. \tag{7}$$

They can also be expressed more compactly in the polar forms $v_i = (v_{m\,i}, \theta_i)$ for individual buses and $V = (V_m, \Theta)$ for a vector of buses. The vectors P_g and Q_g are given as

$$P_g = \left[P_{gen}, P_{es}, P_{LS}\right]^\top \tag{8}$$
$$Q_g = \left[Q_{gen}, Q_{es}, Q_{LS}\right]^\top. \tag{9}$$

The vectors

$$P_{gen} = \left[p_{gen\,1}, p_{gen\,2}, p_{gen\,n_g}\right]^\top \tag{10}$$
$$Q_{gen} = \left[q_{gen\,1}, q_{gen\,2}, q_{gen\,n_g}\right]^\top \tag{11}$$

consist of the real and reactive power, respectively, supplied by each generator. The vectors

$$P_{es} = \left[p_{es\,1}, p_{es\,2}, p_{es\,n_{es}}\right]^\top \tag{12}$$
$$Q_{es} = \left[q_{es\,1}, q_{es\,2}, q_{es\,n_{es}}\right]^\top \tag{13}$$

consist of the real and reactive power, respectively, supplied by each energy storage unit. The vectors

$$P_{LS} = \left[p_{LS\,1}, p_{LS\,2}, p_{LS\,n_b}\right]^\top \tag{14}$$
$$Q_{LS} = \left[q_{LS\,1}, q_{LS\,2}, q_{LS\,n_b}\right]^\top \tag{15}$$

consist of the real and reactive load shed at each bus. They are also expressed in the rectangular forms $s_i = p_i + jq_i$ for individual generators and $S_g = P_g + jQ_g$ for a vector of generators.

The constraints g and h include the network flow constraints as described later in Section II-C. The constraints (4) are of the form

$$v_{m\,i\,\min} \leq v_{m\,i} \leq v_{m\,i\,\max} \tag{16}$$
$$\theta_{i\,\min} \leq \theta_i \leq \theta_{i\,\max} \tag{17}$$
$$p_{i\,\min} \leq p_i \leq p_{i\,\max} \tag{18}$$
$$q_{i\,\min} \leq q_i \leq q_{i\,\max} \tag{19}$$

to impose limits on the voltage magnitude and angle at each bus and the minimum and maximum real and reactive powers of each generator and energy storage unit.

The cost function f is the sum of the costs of conventional generators, energy storage, and load shedding. For the simulations in this article the following cost functions are used:

$$f_{LS}(p_{LS}) = 10 \cdot p_{LS}^2 + 1000 \cdot p_{LS} \tag{20}$$
$$f_{gen}(p_{gen}) = 0.1 \cdot p_{gen}^2 + p_{gen} \tag{21}$$
$$f_{es}(p_{es}) = 0.001 \cdot p_{es}^2. \tag{22}$$

Note that that although the general AC power flow formulation allows for a cost of reactive power, we assume in our simulations that reactive power is essentially free.

The cost f_{LS} represents the value of the lost load, while f_{gen} represents the economic cost of operating the generator. The term f_{es} is a small quadratic cost for the energy storage to ensure that the optimization has a unique solution and will tend to balance the usage of the various storage devices, all else being equal. The marginal cost of using energy storage is less than the marginal cost of using conventional generators, which is less than the marginal cost of load shedding. The primary performance metric is load satisfaction, so the load shedding cost is dominant. The fuel costs are included to encourage fuel minimization if all loads are satisfied. The load demand at each bus is assumed given, and the command for load shedding p_{LS} represents the quantity of power

shortfall at each bus and determines the cost of unserved load $f_{LS}(p_{LS})$. At this early stage of design true economic costs functions are irrelevant. Instead, the costs are chosen heuristically so that the cost of load shed is several orders of magnitude larger than the cost of generation, which is several orders of magnitude larger than the cost of energy storage.

B. MULTI-PERIOD OPTIMAL POWER FLOW

Unlike a single-period optimal power flow which solves for power flow at a single time step only, the MP-OPF optimizes power and energy management for the entire mission simultaneously. The solver has knowledge of all loads during the full mission scenario. One example result is that energy storage units are pre-charged before servicing pulse loads. It is also possible to implement a stochastic version of the multi-period optimal power flow problem [26], but it is not considered here. Conceptually, the MP-OPF is constructed via copies of the candidate power system at each of T time steps. The decision variables V_m, Θ, P_g, and Q_g have a representation at each time step that combine to create the extended MP-OPF decision variables

$$\bar{V}_m = \{V_m(1), V_m(2), \ldots, V_m(T)\} \tag{23}$$

$$\bar{\Theta} = \{\Theta(1), \Theta(2), \ldots, \Theta(T)\} \tag{24}$$

$$\bar{P}_g = \{P_g(1), P_g(2), \ldots, P_g(T)\} \tag{25}$$

$$\bar{Q}_g = \{Q_g(1), Q_g(2), \ldots, Q_g(T)\}. \tag{26}$$

For a power architecture with n_b buses, n_{gen} generators, and n_{es} energy storage (ES) units, the new decision variables $\bar{V}_m$ and $\bar{\Theta}$ each have n_bT elements, and the variables $\bar{P}_g$ and $\bar{Q}_g$ each have $(n_{gen} + n_{es} + n_b)T$ elements.

The time-dependent mission load is assigned for each time step along with power and energy storage capacity constraints. The solver can then make control decisions for the entire mission simultaneously to determine the required power's source and distribution path that minimizes the cost function in (1) and meets the constraints in (2) - (4).

1) GENERATOR RAMP RATES

Conventional gas turbine and diesel generators have both positive and negative power ramp rate limits, defined as r^i_+ and r^i_-, respectively. Their constraints are defined as

$$r^i_- \leq \frac{p^i_t - p^i_{t-1}}{\Delta t} \leq r^i_+, \tag{27}$$

where p^i_t and p^i_{t-1} represent the ith generator power at time t and $t-1$. These generator ramp rates are significantly less than the rate of many advanced pulsed loads, which drives the need for energy storage to service higher rate demands (of typically much shorter duration). Note that although ramp rates on reactive power are possible, they are not considered here.

2) ENERGY STORAGE

Energy storage units can shift power in time but cannot be a net creator of energy, so constraints are added to reflect their storage capacity. We use a basic model for energy storage that does not assume a particular technology and allows for bidirectional power flow.

Each energy storage unit has maximum and minimum real and reactive power limit (e.g. $\pm$ 10 MW and $\pm$ 10 MVAR) and a maximum energy capacity (e.g. 60 MJ). The storage itself is modeled with constant one-way efficiency η_{es} (round-trip η^2_{es}), so the net power after losses is integrated to determine the energy storage state,

$$E_{min} \leq E_{start} - \sum_{t=0}^{\tau} p_{es-net_j}(t)\Delta t \leq E_{max} \quad \forall \tau \in (0, T), \tag{28}$$

$$p_{es-net_j}(t) = \begin{cases} \eta_{es} p_{es_j}(t) & p_{es_j} \leq 0 \\ \frac{1}{\eta_{es}} p_{es_j}(t) & p_{es_j} > 0 \end{cases} \tag{29}$$

where $p_{es_j}(t)$ is the power from the jth energy storage unit (positive for output power), and p_{es-net_j} is the net power stored internally after losses. For simplicity, it is assumed that the energy storage unit can supply its rated reactive power with no effect on the stored energy. In reality, there will be an energy loss associated with supplying reactive power. These tend to be much smaller, however, because they are driven primarily by the converter efficiency. The time step is Δt, and E_{min} and E_{max} are the minimum and maximum stored energies, respectively. Some storage technologies degrade over time, so these power and capacity values are based on those available throughout the useful life of the storage devices.

Additionally, we add the constraint

$$\sum_t p_{es-net_j}(t)\Delta t = 0 \tag{30}$$

to set the cumulative sum of energy in each storage unit to zero in order to ensure that the charge returns to its initial value. Otherwise, the optimal solution could result in a depleted energy storage state with insufficient reserves for future load demand beyond the final time of the simulation. We assume all energy storage units are fully re/dis-chargeable without degradation and the cost for accessing it is virtually zero.

In reality, energy storage units have rate limits too, but they are much faster than a generator's and the simulation time step, so they are considered infinite. In setting up the optimization problem, the generator ramp rate and energy storage constraints (27)-(28) are added as linear inequality constraints (3) and the energy storage terminal constraints (30) are added as linear equality constraints (2).

3) MULTI-PERIOD OBJECTIVE FUNCTION

After adding the multi-period constraints on energy storage capacity and ramp rates, the final formulation for multi-period optimal power flow is modified from (1) as

$$\min_{\bar{x}} \bar{f}_{gen}(\bar{P}_g) + \bar{f}_{es}(\bar{P}_{es}) + \bar{f}_{LS}(\bar{P}_{LS}) \tag{31}$$

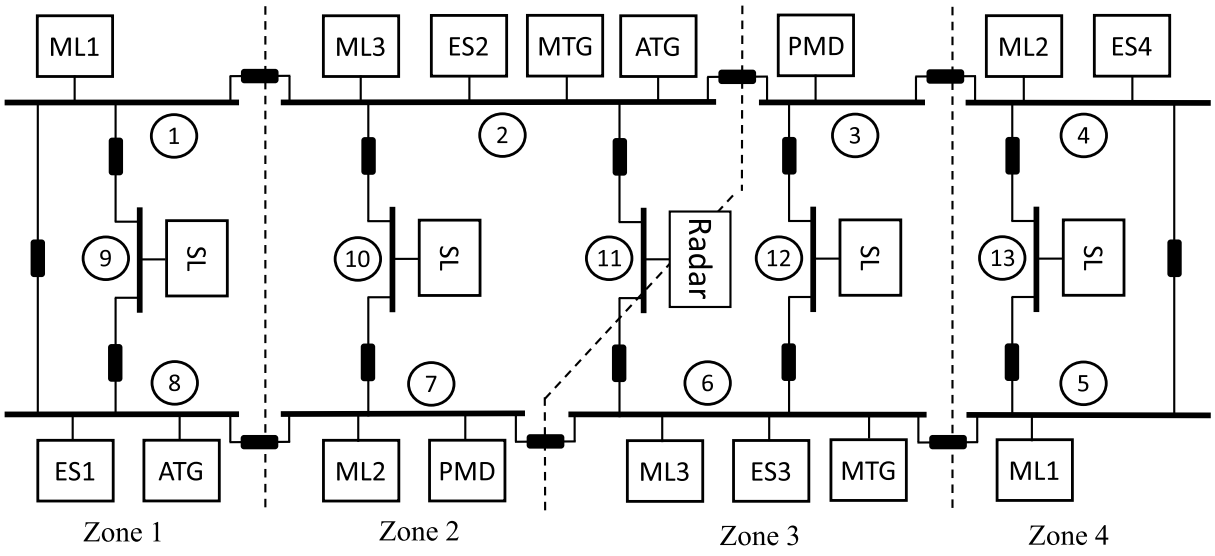

FIGURE 2. The representative thirteen-bus power system architecture has 8 switchboards, 5 load centers, and 4 zones with numbered buses as shown (reproduced from [37]). Components include two Main Turbine Generators (MTG), two Auxiliary Turbine Generators (ATG), four energy storage units (ES), four Service Loads (SL), two Propulsion Motor Drive (PMD) loads, one Radar (R) load, and three Mission Loads (ML1, ML2, ML3).

where the decision variables $\bar{x} = \left[\bar{V}_m, \bar{\Theta}, \bar{P}_g, \bar{Q}_g\right]^\top$, costs, and constraints are all modified to the multi-period extended versions by considering copies of the candidate power system at each of T time steps as described above. The optimization then determines these decision variables across all T time steps.

For further details on the multi-period optimal power flow formulation see [26] and [25].

C. NETWORK FLOW CONSTRAINTS

1) AC POWER FLOW

The network power flow equations are dictated by basic circuit laws. Using the notation in [24]

$$I_{bus} = Y_{bus} V \tag{32}$$

where the complex bus admittance matrix Y_{bus} relates the complex node voltages V to the complex nodal current injections I_{bus}. The complex power injection at each bus $S_{\text{bus}} = P_{\text{bus}} + jQ_{\text{bus}}$ can then be expressed as

$$S_{\text{bus}}(V) = [V] I^*_{\text{bus}} = [V] Y^*_{bus} V^* \tag{33}$$

where $[\cdot]$ is an operator that converts a vector to a diagonal matrix and $*$ denotes complex conjugate. Power balance at each bus then dictates

$$g_P(\Theta, V_m, P_g) = P_{\text{bus}}(\Theta, V_m) + P_{\text{total}} = 0 \tag{34}$$
$$g_Q(\Theta, V_m, Q_g) = Q_{\text{bus}}(\Theta, V_m) + Q_{\text{total}} = 0 \tag{35}$$

where P_{total} and Q_{total} are vectors of total real and reactive power injections at each bus. They represent the net load injection (load demand minus load shed) at each bus minus the power supplied by all generators and energy storage units connected to each bus. These power balance constraints then form the equality constraints (2).

Likewise, the currents injected at the "from" and "to" ends of a line, I_f and I_t, can be expressed as [24]

$$I_f = Y_f V \tag{36}$$
$$I_t = Y_t V \tag{37}$$

where Y_f and Y_t are the "from" and "to" admittance matrices, respectively. Equations (36) and (37) can then be written in terms of complex power flows as

$$S_f(V) = [C_f V] I^*_f = [C_f V] Y^*_f V^* \tag{38}$$
$$S_t(V) = [C_t V] I^*_t = [C_t V] Y^*_t V^* \tag{39}$$

where C_f and C_t are matrices of zeros and ones mapping buses to the branches that they are connected from and to, respectively. Given these complex power flows, the constraints on apparent power flow can then be expressed as

$$h_f(\Theta, V_m) = |S_f(\Theta, V_m)| - S_{\max} \leq 0 \tag{40}$$
$$h_t(\Theta, V_m) = |S_t(\Theta, V_m)| - S_{\max} \leq 0 \tag{41}$$

where $S_{\max}$ is a vector of the maximum line apparent power flows, to form the inequality constraints (3).

2) DC POWER FLOW

In certain cases the network flow equations can be simplified by using the DC (linear) approximation to the optimal power flow. The DC approximation makes the following assumptions [43]:

- All lines are lossless.
- All bus voltage magnitudes are 1 p.u.
- All voltage angle differences across branches are small.

Based on these assumptions, it can be shown that the bus power injection (33) simplifies to [24]

$$P_{\text{bus}}(\Theta) = B_{\text{bus}} \Theta \tag{42}$$

where B_{bus} is a matrix formed from the line reactances. The power balance constraint (34) can then be simplified to

$$g_P(\Theta) = B_{\text{bus}}\Theta + P_{\text{total}} = 0. \tag{43}$$

The line flows (38) and (39) can also be simplified to [24]

$$P_f(\Theta) = -P_t(\Theta) = B_f\Theta. \tag{44}$$

This allows the inequality constraints (40) and (41) to be simplified to

$$h_f(\Theta) = B_f\Theta - P_{\max} \leq 0 \tag{45}$$
$$h_t(\Theta) = -B_f\Theta - P_{\max} \leq 0 \tag{46}$$

A limitation of the DC power flow approximation is that it only solves for real power. Even when the real power demands are below generator power limits, the generators still may not be able to provide adequate reactive power. Additionally, lines that are not overloaded in terms of real power may be overloaded in terms of apparent power. Therefore, the DC approximation must be used with cognizance that real power demands are the dominating effects. See Section III-C for a validation of these assumptions for our particular system.

3) NETWORK RECONFIGURATION

Generators and loads determine the current injections on each bus, but only indirectly change the power flow on lines. Lines with power converters to directly control flow can be represented using an additional decision variable. Line limits are included as hard constraints in (40) and (41) to reflect overheating or breaker tripping. When these constraints are active it typically indicates an undersized power transfer system that cannot move power to where it is needed. However, a single line can overload even while other lines have excess capacity.

A given scenario might result in nominal load shortfall due to constraint violation, but in reality the system can still complete the mission once a breaker trips. This often occurs if there are multiple power paths, but some have limited capacity. A simple example is a port and starboard bus system as shown in Fig. 3, with a vital load on bus 9 dually fed from both buses. These feeders for bus 9 may have a rating to serve only the vital load, but can act as an unintended power transfer path between buses 1 and 8 and overload. If one of these breakers opens on the lower-rated path, all the buses and loads can be fully served with no overloads.

Transmission system reconfiguration by opening breakers allows for different sets of permissible generator power outputs and can improve overall capacity. However, determining multiple admissible configurations is a difficult problem - especially when considering voltage limits and transients [29], [44], [45] - and is therefore not considered in this setup.

III. EXAMPLE POWER SYSTEM

A. POWER SYSTEM ARCHITECTURE

This article uses a thirteen-bus shipboard system, as shown in Fig. 2. The model is based on a notional all-electric ship

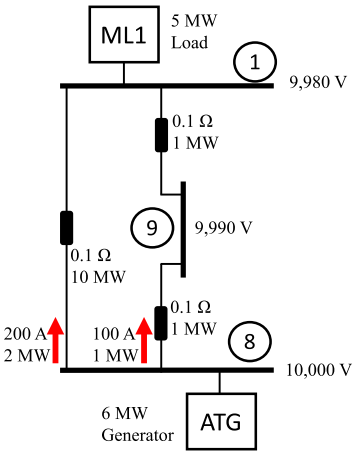

FIGURE 3. A simple example of network flow constraints in a DC system, where load shedding occurs despite available generation and nominal transmission capacity. This portion of the full system in Fig. 2 shows a 6 MW Auxiliary Turbine Generator (ATG) on bus 8 connected to a 5 MW load on bus 1 through a line of 10 MW capacity, which is normally sufficient. However, there is a second 1 MW path through bus 9, which is at its limit. In this configuration there is no way to increase power flow through the larger line as any change in bus voltage will overload the low capacity path, so the load receives less than 3 MW.

TABLE 1. Power system parameters. The Rating (1 p.u.) column indicates the baseline (per unit) rating for each parameter. The sweep range indicates the range that the parameter can be swept over with respect to the baseline value.

Parameter	Rating (1 p.u.)	Units	Sweep Range (p.u.)
MTG Max Power	35	MW	0.8-1.2
ATG Max Power	6	MW	0.8-1.2
Gen Ramp Rate	±1	MW/s	0.1-1.5
Storage Power	±10	MW	0.2-1.0
Storage Energy	60	MJ	0.0-6.0
Storage Efficiency	100	%	0.5-1.0
Line Limits	41	MVA	0.35-2.0

developed by the Electric Ship Research and Development Consortium (ESRDC) [46]. The model has undergone a series of revisions [25], [34] to reach its present form [37]. It is a four-zone power and energy architecture with two Main Turbine Generators (MTG), two Auxiliary Turbine Generators (ATG), and four energy storage (ES) units (one per zone). There are 6 main load types distributed throughout the ship: 4 evenly distributed Service Loads (SL), 2 Propulsion Motor Drive (PMD) loads each with 1/2 of the total propulsion load, 1 Radar (R) load, and 3 pairs of Mission Loads (ML1, ML2, and ML3).

Table 1 shows total power generation is 82 MW, comprised of two 35 MW MTGs and 2 ATGs at 6 MW each. Four 10 MW/60 MJ energy storage units add an additional 40 MW of power and 240 MJ of energy storage. The baseline parameter values are taken from [25], and the sweep range parameter is used for the trade studies in later sections. Load shedding is allowed on each bus to guarantee feasibility as mentioned in Section II.

Power conversion modules are omitted as they can be represented as a branch power limit and a small line loss. For the case studies in this article, all such losses (along with line losses) are omitted. This is because at an early design stage losses are typically not known [25]. In the detailed design

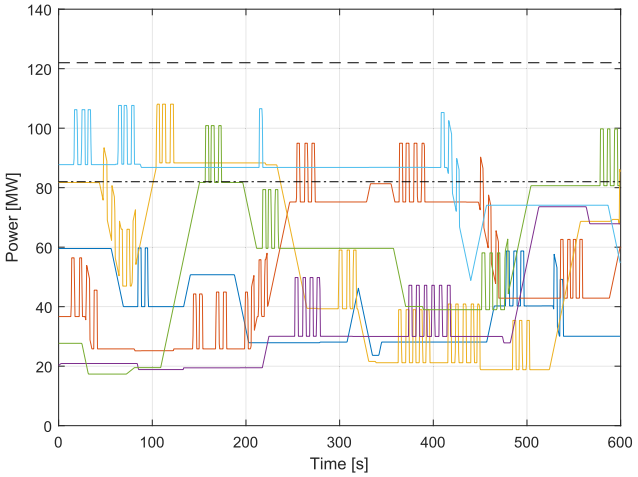

FIGURE 4. Sample mission load profiles showing the time-sequenced total ship load demand required to accomplish representative operational missions. Each solid trace indicates a single load profile. Each load profile is formed from the combination of constant and pulsed load demands of various powers, ramp rates, and time durations. Note the large variation in load demand both within and across missions. Dashed horizontal lines show the 82 MW total generation capacity and 122 MW total power available including energy storage.

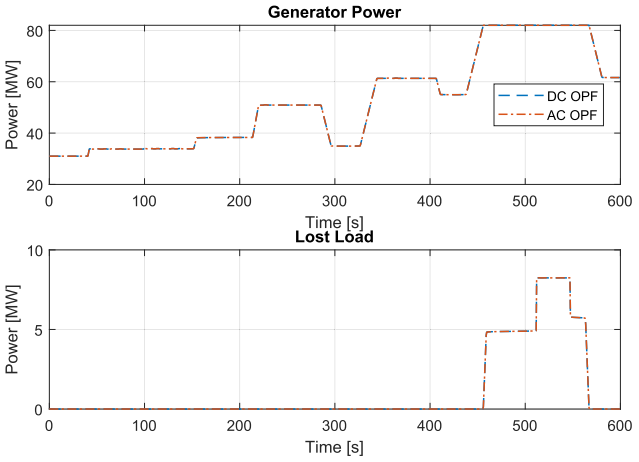

FIGURE 5. Comparison of AC and DC optimal power flow formulations. The top plot shows generator power summed over all four generators. The bottom plot shows lost load. The two solutions agree to within 650 kW.

phase, the upper bound established in the preliminary phase can be used as a benchmark to evaluate the losses associated with actual lines, power converters, and energy storage units.

Because energy storage losses are typically higher than generation or transmission losses, they are a major driver of the overall system efficiency. The system efficiency is also heavily mission-dependent. For instance, in a mission where high-efficiency generators are the primary power source, the mission efficiency will be very high. Conversely, a mission that must heavily rely on low-efficiency energy storage will have a much lower mission efficiency.

B. OPERATIONAL MISSION LOAD PROFILE

This ship system (Fig. 2) is evaluated for its ability to supply power to 200 samples of various operational mission load profiles generated from a load demand model [34], [47]. These mission load profiles each represent a single tactical engagement over 600 s, which is sufficient time to fully exercise the power system via energy storage charge discharge, generator ramping, etc. Fig. 4 shows the time-dependent load demand profiles of five such trials. (The five trials were chosen to illustrate the large variation on load demand both within and across trials.) Given the system capabilities, we would like to identify which scenarios fail, and to what extent. A failed scenario means that the system is physically incapable of supplying the full load without violating constraints, regardless of the controller selected. For this study, a failed scenario is defined as any trial that must shed load, regardless of how much or for how long.

C. SOLUTION METHOD

The power system solver MATPOWER [24] is used, which accepts problems in standard form (1)-(3). This solver can handle the MP-OPF problem by using the extended MP-OPF variables (31). Time steps of 0.5 s are used for Δt in (28)-(30). This framework allows full AC power flow analysis; the results here use the DC approximation to improve solution speed while producing nearly identical results.

To test whether the DC approximation is valid for the example system in Fig. 2, several representative load profiles were run using both AC and DC optimal power flow. Two major simplifying assumptions are made in this set up. First, lines are modeled as lossless, with a resistance of 0.0 p.u. and a reactance of 0.01 p.u. This is not a major limitation for a ship system because cables on ships are very short compared to transmission lines in terrestrial systems. The second is that all loads have unity power factor. This is also not a major limitation as ship designers have tight control over what loads are placed on ships and can therefore require that loads with low power factors include appropriate power factor correction.

Fig. 5 shows an example for one profile. For this particular profile, the AC and DC MP-OPF results are nearly identical. The maximum difference in generator real power is 650 kW. For the AC system, the maximum generator reactive power supplied is 12.9 kVAR and the maximum line reactive power flow is 34.7 kVAR. Also, the bus voltage magnitudes are all equal to 1.0 p.u. to 3 significant digits. These results indicate that for our particular system the DC approximation is quite accurate. The DC approximation solved in 27 minutes 55 seconds while the AC solution took 29 minutes and 5 seconds to converge to a solution. Due to the difference in solution speeds, all of the following results use the DC power flow approximation.

IV. EXAMPLE OPTIMIZATION RESULTS

To study the trade offs between different component specifications, a set of power systems are generated with varying specifications using the same architecture as the baseline system in Fig. 2. A single mission load profile (as in Fig. 4) is applied to the set of systems to demonstrate the behavior

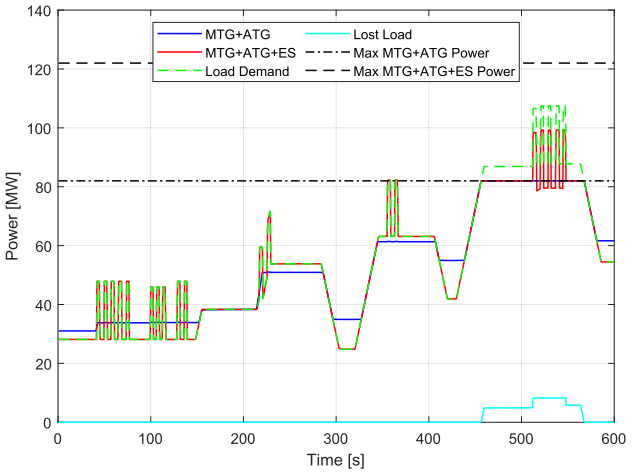

(a) Total generator and storage power vs. load demand for a representative mission with 41-MW line limits and 1 MW/s generator ramp rate limits. The system fails to meet the load demand between 455 s and 570 s.

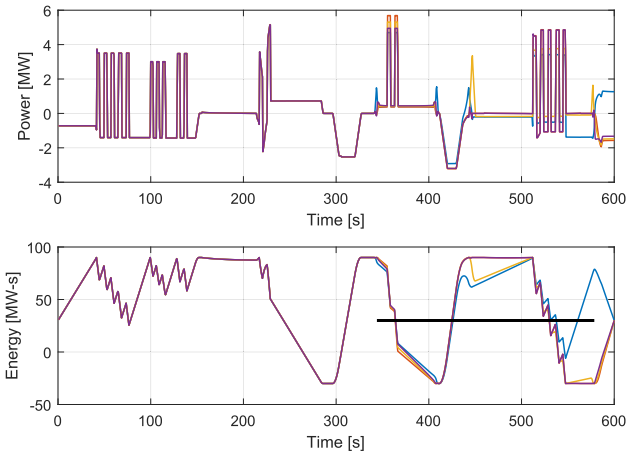

(b) Energy storage power and energy for the 4 ES units with 14 MW line limits. Each solid trace shows a distinct energy storage unit. The thick horizontal line indicates the duration of an active line limit constraint.

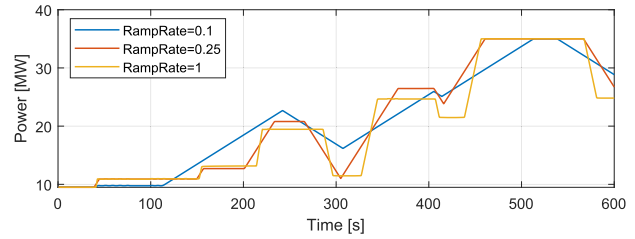

(c) MTG power with varying ramp rates in MW/s. Energy storage must absorb the large load changes where MTG ramp rates are too low.

FIGURE 6. Typical system performance (a) compared with the effects of limited power flow (b) and generator ramp limits (c). Energy storage unit capacities are 60 MJ each. The system cannot fully meet demand and sheds load from 455-570 s in the baseline case (a). Energy storage usage is similar even with reduced line limits (b), but the normally identical units start to diverge based on location once there is an active flow constraint. The generator usage is aggressive with the baseline 1 MW/s limits (c), but the response slows with limited ramp rates.

of the multi-period power flow optimization algorithm as shown in Fig. 6. This method was initially used on a similar power system without line flow or ramp rate constraints [25], so this section focuses on the effects of including them.

A. RESULTS WITH HIGH RAMP RATES AND LINE LIMITS

As a first case, we consider the baseline system with all generator ramp rates set to 1 MW/s and all line flows set to 41 MW. The results for a typical 600-second mission vignette are shown in Fig. 6a. With the line limits set to half of the total generator capacity, power flow constraints are not active and the load demand stays below the total installed power (i.e. generators plus storage). However, even with the high generator ramp rates and line limits, the load can not be fully met due to the limited energy storage capacity.

At the beginning of the mission in Fig. 6a the generators provide more power than the load demand in order to charge the energy storage units. Then, during a period of load spikes, generator power remains relatively constant while energy storage supplies the load until demand exceeds the total generator power (as seen by the nonzero value of lost load from 455-570 s). At this point, the system sheds some of the load in order to reserve stored energy for the large load spikes. This is because the cost of load shedding is quadratic; therefore the system incurs a lower cost by having a smaller shortfall for a longer time rather than a larger shortfall for a shorter time.

Fig. 6a illustrates why analyzing system performance is much more complicated than simply ensuring that total load demand is less than total installed generation and energy storage capacity. Factors such as generator ramp rates and energy storage capacities must also be accounted for. Additionally, when there is a shortfall, the optimal method for addressing the shortfall (i.e. by shedding load) must be carefully considered.

B. EFFECTS OF RESTRICTIVE LINE LIMITS

The same load profile in Fig. 6a is applied to the baseline system with its line limits reduced to 14 MW. The energy storage behavior is shown in Fig. 6b.

When the line limits are reduced, the line constraints become active and change the way the power sources are allocated. The four energy storage units behave symmetrically until diverging when restrictive line limits are active. The limits create a location-based value for the different generation assets, often termed locational marginal pricing. Fig. 6b also indicates when the line limit constraints are active as determined by a non-zero value of the Lagrange multiplier outputs of the solver. This constraint causes the four storage units to diverge.

A major takeaway from Fig. 6a is that when line power flow limits are high, the location of energy storage is not significant since all units are utilized equally regardless of location. If, however, flows are constrained, energy storage placement becomes important. Also note that energy storage placement may be influenced by other factors. For instance, if line losses are high, energy storage should be physically close to loads. Also, it may be necessary to locate energy storage in different parts of the ship due to survivability concerns.

C. RESULTS WITH LIMITED GENERATOR POWER RAMP RATES

Most generators have power ramp rates that are insufficient to serve advanced pulse loads. Fig. 6c shows the effect of varying generator ramp rates on the baseline mission. When ramp rate limits are high, the generators are able to quickly ramp to track large changes upward or downward in load. When ramp rate limits are lower, however, generators must increase their generation early in anticipation of large load spikes. (This is particularly prominent in the trace for the 0.1 MW/s ramp rate, which is constantly ramping up or down at its maximum rate in anticipation of future load demands.) Excess power generation will be used to charge energy storage, which will then aid the generator in servicing large load spikes. This means that, all else being equal, a system with low generator ramp rates will place a higher demand on energy storage than a system with high generator ramp rates.

D. OTHER CONSIDERATIONS

In many cases it is not a single constraint that causes a load shortfall, but the interaction of multiple constraints. For example, a mission that is unsuccessful in meeting the load demand with restrictive line flow and ramp rate constraints may be successful if either constraint is relaxed slightly. Therefore if a mission fails, all active constraints must be considered together to determine the root cause. This analysis should include potential transmission reconfigurations as mentioned in Sec. II-C3, which are not automatically optimized.

V. TRADE STUDIES

The proposed method can rapidly create data for trade studies between different power system designs. Performance is controller dependent, so this upper bound method is a useful way to compare two candidate systems. Although this best case is unrealizable without exact future knowledge, it can provide insights into the relative performance of designs.

Performance on a single mission is not always insightful, so we consider a set of 200 representative mission load profiles. A mission is considered a ''success'' if all the load demands are met at all times, and a ''failure'' if not. There is some middle ground that can be quantified by MW-hrs of unserved load or similar metrics, but these can be difficult to translate into mission success and therefore are not considered in this study. Data is generally presented as a percentage of successful missions. This approach provides the ship designer with clear insight into which missions are attainable (or not). In the failed mission case, it also enables them to take a closer look at how critical those missions are and which loads may be shed.

These multi-dimensional results are organized as specific design decisions of interest between particular variables. All trade studies are conducted using the system shown in Fig. 2 using the parameter values in Table 1 as a baseline, with variations shown in per unit (p.u.) with respect to this baseline. The sweep range is meant to encompass the range of values from minimum to maximum capability.

A. DESIGN DECISIONS

1) ENERGY STORAGE TECHNOLOGY

When determining they type of energy storage to install designers must take into account energy storage power, capacity, and efficiency. Fig. 7a shows the mission success rate as a function of energy storage capacity and power. Increasing the storage capacity is initially valuable, but becomes less useful unless power limits are also increased. However, increasing energy storage power beyond 0.75 p.u. provides no additional performance. Other factors also influence this decision, including robustness to line outages.

Fig. 7b shows the relationship between energy storage power and efficiency while energy storage capacity is held constant at 1 p.u. The figure illustrates that if energy storage is very inefficient (below 70% one-way) performance will be degraded. For moderate efficiencies (between 80% and 90%) the percentage of missions that can be successfully accomplished drops by only 1% from the 100% efficient case. For very high efficiencies (above 95%) there is no degradation in performance for storage powers greater than 0.75 p.u.

Fig. 7c illustrates the tradeoff between energy storage capacity and efficiency while energy storage power is held constant at 1 p.u. Not surprisingly, for low storage capacities, efficiency is not a major concern. This can be seen by the fact that contours of constant performance are nearly vertical for capacities less than 1 p.u. At higher capacities, efficiency matters much more. For instance, at 4 p.u. of storage capacity only 77% of missions are successful when storage efficiency is 50%. For the same capacity, if efficiency is increased to 85%, then 84% of missions are successful.

These results indicate that if the only free design parameter is the type of energy storage, decreasing storage power to 0.75 p.u. and increasing capacity will yield better performance for the same size/weight/cost. Likewise, energy storage should ideally be at least 90% to 95% efficient. Higher efficiencies than this could save energy and lower operating costs, but do not yield a meaningful increase in the percentage of missions that can be accomplished. As shown below, varying both generator and energy storage parameters yields more options.

2) ENERGY STORAGE CAPACITY VS LINE LIMITS

Fig. 7d shows the percentage of missions that are successful as a function of energy storage capacity for several different line limits. Inadequate line limits can be compensated with energy storage. For instance, the system with 4.0 p.u. of energy storage and a line limits of 0.45 p.u. has similar performance to the system with 1 p.u. of energy storage and a line limit of 1.0 p.u. Note, however, that for the system with line limits of only 0.35 p.u. increasing energy storage does not significantly improve performance. For a fully functional power system there is no performance gained by increasing the line limit beyond the baseline 1.0 p.u. There may be additional benefits if system components are damaged or off-line, which is not considered here.

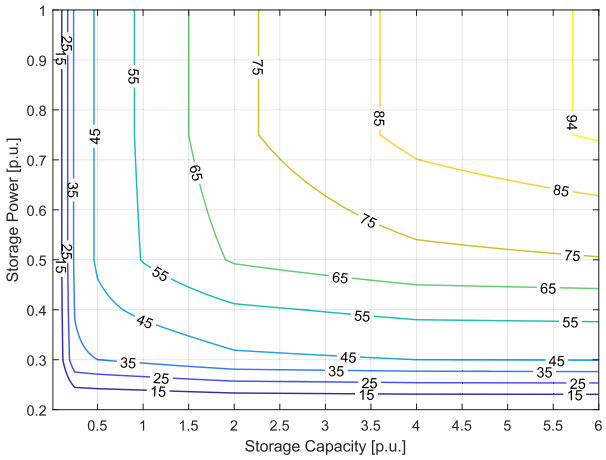

(a) Mission success as a function of energy storage capacity and power.

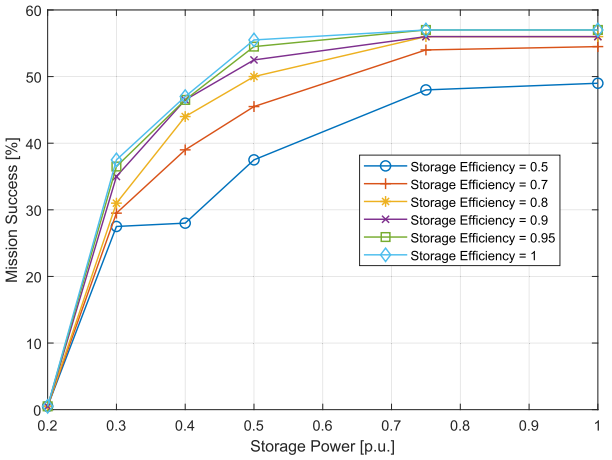

(b) Mission success as a function of energy storage power and efficiency.

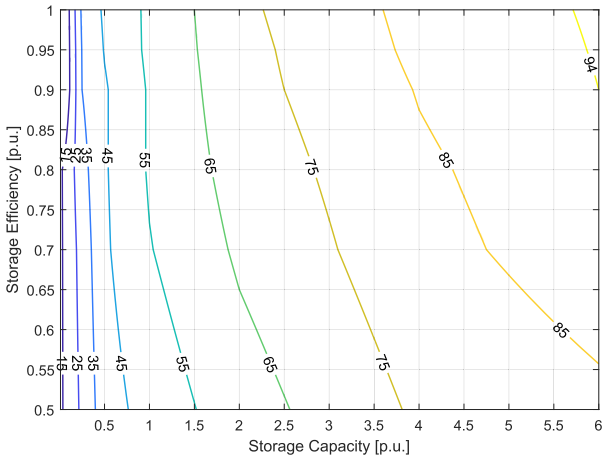

(c) Mission success as a function of energy storage capacity and efficiency.

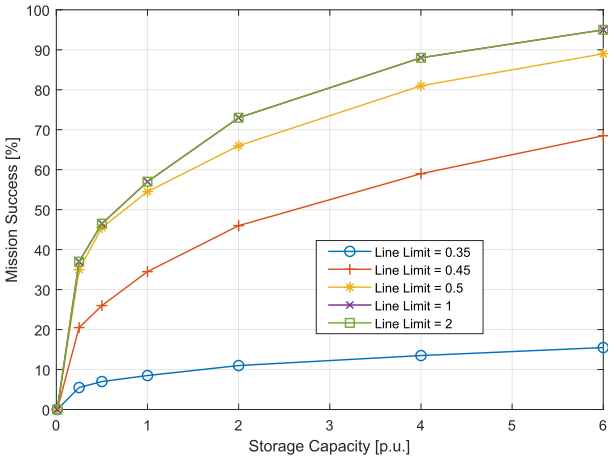

(d) Mission success as a function of energy storage capacity and line flow limits.

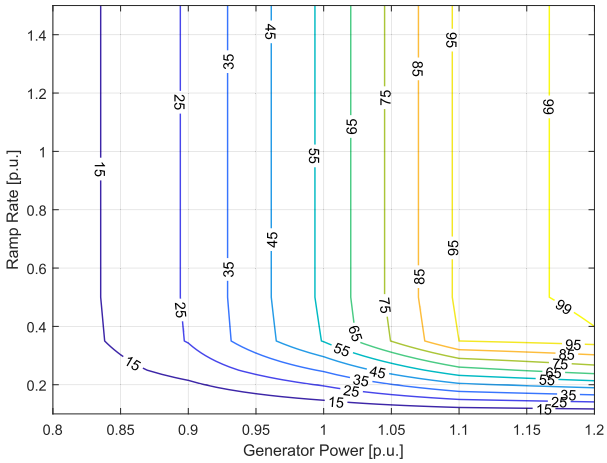

(e) Mission success as a function of generator power and ramp rate.

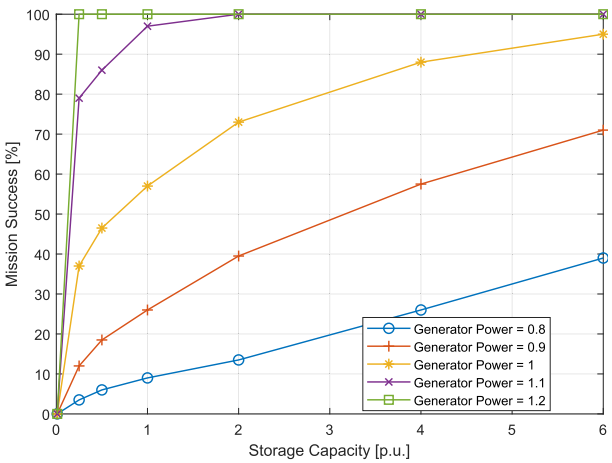

(f) Mission success as a function of energy storage capacity and generator power.

FIGURE 7. **Trade studies showing the relationship between system parameters and the percentage of missions that are successful. Figs. 7a, 7c, and 7e show contours of the Pareto frontier using interpolated data. Figs. 7b, 7d, and 7f show the raw data from the parameter sweeps. In each plot all parameters other than the two being swept are held constant at 1 p.u. Efficiencies are one-way (round-trip would be η_{es}^2).**

3) GENERATOR RAMP RATE VS PEAK POWER

Fig. 7e illustrates the relationship between generator power and ramp rate. For any given generator power level, performance increases with ramp rate up to 0.5 p.u., beyond which there is little improvement. Likewise, for a given ramp rate, performance increases with generator power until a generator power of approximately 1.2 p.u.

From these results, it is clear that the baseline generator set is not optimal for the system's mission requirements, with less than 60% mission success. That could be improved to

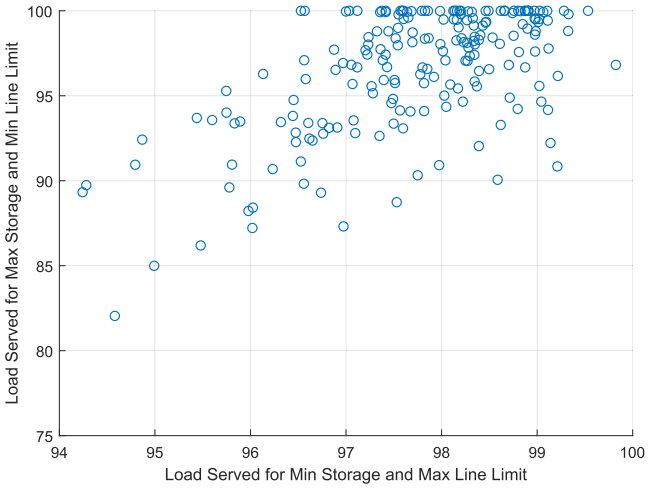

(a) System with minimum energy storage capacity and maximum line limit (x axis) vs. system with maximum energy storage capacity and minimum line limit (y axis).

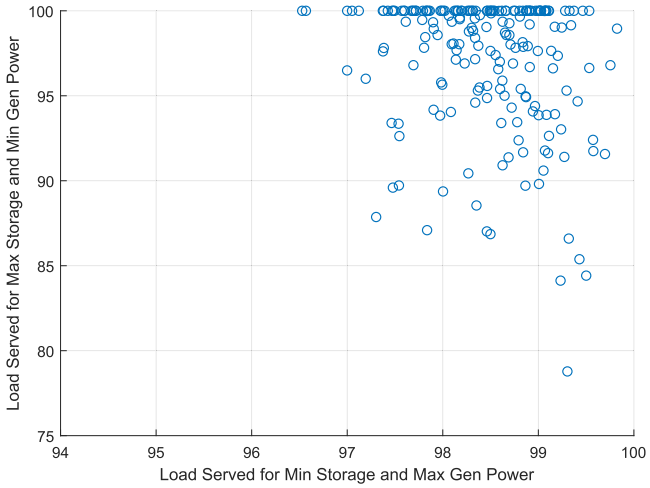

(b) System with minimum energy storage capacity and maximum generator power (x axis) vs. system with maximum energy storage capacity and minimum generator power (y axis).

FIGURE 8. Relative difficulty of completing various missions. Each plot compares the percentage of load served by mission for two different configurations. Each point represents a single mission, and shows its relative difficulty for both cases.

over 95% with a set of generators with 1.1 p.u. of power, but only 0.5 p.u. of ramp rate. Similar studies could consider only one generator or generator type.

4) BETTER GENERATORS VS ENERGY STORAGE CAPACITY

Fig. 7f shows the impact of both generator power and energy storage capacity, including combinations that result in 100% mission success. Previously, when considering generator modifications alone (Fig. 7e), a generator power of 1.2 p.u. is required to accomplish all missions. This same result can be achieved with only 1.1 p.u. by increasing the storage capacity to 2 p.u.

B. ADDITIONAL PERFORMANCE METRICS

The percentage of missions that meet the load demand throughout is not the only design metric that may be considered. Others include the percentage of load served (defined as the load energy served divided by the energy demand), an assigned cost of load shed, or the percentage of time that all the loads are served.

As a comparison example, with a generator power of 0.8 p.u. and no energy storage, all missions shed some load and fail, but over 90% of the load is still served. If there were a design requirement to serve 99% of the load, it could be achieved with a generator power of 1 per unit and an energy storage capacity of 0.25 per unit. From an uptime perspective, all loads are served 90.5% of the time in this case.

These results taken together illustrate how one must choose the appropriate performance metric for the given design problem. In general Mission Success $\leq$ Percent of Uptime $\leq$ Percent of Load. Therefore requiring 99% mission success may be a much more stringent requirement than requiring 99% of load served. In the case of a warship engagement scenario, any interruptions to certain critical loads is unacceptable; therefore, percentage of successful missions is the primary metric considered here.

C. SHADOW PRICES

The Kuhn-Tucker multiplier associated with an inequality constraint on the power flow problem represents the reduction in cost that could be achieved by relaxing the constraint. (Inactive constraints will have zero cost.) In the multi-period problem these change with time, so they can provide insight into which constraints are binding at different times in the mission.

D. SPREAD IN PERFORMANCE BY MISSION

This subsection considers the variability of performance among the 200 different missions. In particular, we study if the missions have the same relative difficulty for different ship configurations. To do this, each mission's difficulty is evaluated in terms of percentage of load served for two very different configurations. A scatter plot is then generated, showing the percentage of load served by mission for each configuration.

Fig. 8a shows one such plot comparing two potential architectures. The first architecture has low energy storage capacity (0.01 p.u.) and high line limits (2.0 p.u.), while the second architecture has high energy storage capacity (6.0 p.u.) and low line limits (0.35 p.u.). Points in the lower left corner of the plot represent missions that are difficult for both architectures and points in the upper right corner those that are easy for both. Most points are along a diagonal line from the lower left to the upper right. This trend indicates that even though the architectures have different performance in an absolute sense, they find the same missions relatively difficult.

Fig. 8b compares two other architectures. The first architecture has low energy storage capacity (0.01 p.u.) and high generator power (1.2 p.u.), while the second has high energy storage capacity (6.0 p.u.) and low generator power (0.8 p.u.). The points are dispersed relatively uniformly in this case, indicating runs that are relatively stressing for one architecture, but easy for another. For instance, the mission in the

upper left corner has only 96.5% of load served by the first architecture, but has 100% served by the second architecture. Conversely, the point in the lower right has 99.3% of load served by the first architecture, but only 78.8% of load served by the second architecture. This illustrates why analyzing only the ''difficult'' missions is generally not sufficient except in particular cases like Fig. 8a.

VI. DISCUSSION

Power systems with energy storage and generator dynamics are typically difficult to analyze because they require a new system controller for every candidate system architecture, a time consuming process which can provide erroneous results without careful controller design. The methods in this article produce a best-case upper bound performance for a given architecture. This is particularly valuable for early stage trade studies conducted well before the design of specific system controllers

The method is automated and allows for large scale architecture trade studies with minimal human input as illustrated in Fig. 1, where the amount of lost load would typically act a fitness metric for the system.

The technique is also useful to a human designer to gain insight and quantitative comparisons. Three example use cases are discussed in this article:

- The system behavior on a single mission as shown in Fig. 6 provides insight into the time and location of power shortfalls and transmission congestion, as well as typical generator and storage utilization.
- The type of trade study data shown in Fig. 7 provides quantitative, actionable insight. For this nominal system design, the data in Fig. 7a would encourage a shift to storage devices that have higher capacity but lower power, e.g. batteries rather than capacitors. Similarly, Fig. 7e demonstrates that for the nominal 1 p.u. design point, generator ramp rate should be sacrificed in favor of generator power.
- Any conclusions are based on the mission load scenarios, so the upper bound performance can identify which missions are fundamentally difficult and dominating the design process, as shown in Fig. 8.

VII. CONCLUSION

A daunting task for ship designers is analyzing complex shipboard power architectures with constraints and time dependent elements like generator ramp rates and energy storage. This is particularly problematic early in the design process because each candidate power system architecture can only be evaluated by designing a controller for it, which is time consuming and subject to variations based on design choices.

The technique developed in this article produces a quantifiable upper bound on the best case performance of *any* possible controller for a power system, and indicates fundamental limitations of the architecture itself. Real controllers may not achieve this upper limit because the analysis here assumes exact future load knowledge, but it provides a well-defined upper bound for use as a standard method to compare architectures. For early-stage system analysis before the actual controllers are designed, the eventual system performance can be estimated by considering this upper limit and the lower bound of a purely instantaneous controller with no future predictions.

In contrast to previous work, this method solves a dynamic optimization problem accounting for energy storage capacity and generator ramp rates in addition to generator and energy storage powers and line flow limits. The problem is formulated as a nonlinear multi-period optimal power flow optimization with additional linear constraints, and solved via numerical optimization. The power shortfall at each bus for a given mission is quantified, which can assist in prioritizing possible capability improvements.

The proposed method has been demonstrated on a notional electric warship using a set of mission load profiles. Results indicate that significant performance gains can be achieved with minor improvements to the baseline system. For instance, a 10% gain in performance can be achieved by choosing an energy storage technology that has double the storage capacity and half the peak power of the baseline technology. Likewise, mission performance can be increased by 35% with a 10% increase in generator power, even if generator ramp rates are halved. Through considering both generation and storage simultaneously the performance can be improved from under 60% to nearly 100% with a 10% increase in generator power and a doubling of energy storage capacity.

REFERENCES

[1] G. Sulligoi, A. Vicenzutti, and R. Menis, ''All-electric ship design: From electrical propulsion to integrated electrical and electronic power systems,'' *IEEE Trans. Transp. Electrific.*, vol. 2, no. 4, pp. 507–521, Dec. 2016.

[2] E. Skjong, R. Volden, E. Rødskar, M. Molinas, T. Arne Johansen, and J. Cunningham, ''Past, present, and future challenges of the marine Vessel's electrical power system,'' *IEEE Trans. Transp. Electrific.*, vol. 2, no. 4, pp. 522–537, Dec. 2016.

[3] R. R. Chan, S. D. Sudhoff, and E. L. Zivi, ''An approach to optimally allocate energy storage in naval electric ships,'' in *Proc. IEEE Electric Ship Technol. Symp.*, Apr. 2011, pp. 402–405.

[4] M. Falahi, K. L. Butler-Purry, and M. Ehsani, ''Reactive power coordination of shipboard power systems in presence of pulsed loads,'' *IEEE Trans. Power Syst.*, vol. 28, no. 4, pp. 3675–3682, Nov. 2013.

[5] W.-S. Im, C. Wang, L. Tan, W. Liu, and L. Liu, ''Cooperative controls for pulsed power load accommodation in a shipboard power system,'' *IEEE Trans. Power Syst.*, vol. 31, no. 6, pp. 5181–5189, Nov. 2016.

[6] D. J. Singer, N. Doerry, and M. E. Buckley, ''What is set-based design?'' *Nav. Eng. J.*, vol. 121, no. 4, pp. 31–43, Oct. 2009.

[7] E. A. Sciberras, B. Zahawi, D. J. Atkinson, A. Breijs, and J. H. van Vugt, ''Managing shipboard energy: A stochastic approach special issue on marine systems electrification,'' *IEEE Trans. Transp. Electrific.*, vol. 2, no. 4, pp. 538–546, Dec. 2016.

[8] P. Kankanala, S. C. Srivastava, A. K. Srivastava, and N. N. Schulz, ''Optimal control of voltage and power in a multi-zonal MVDC shipboard power system,'' *IEEE Trans. Power Syst.*, vol. 27, no. 2, pp. 642–650, May 2012.

[9] M. R. Hossain and H. L. Ginn, "Real-time distributed coordination of power electronic converters in a DC shipboard distribution system," *IEEE Trans. Energy Convers.*, vol. 32, no. 2, pp. 770–778, Jun. 2017.
[10] T. V. Vu, D. Gonsoulin, F. Diaz, C. S. Edrington, and T. El-Mezyani, "Predictive control for energy management in ship power systems under high-power ramp rate loads," *IEEE Trans. Energy Convers.*, vol. 32, no. 2, pp. 788–797, Jun. 2017.
[11] H. Iranmanesh and A. Afshar, "MPC-based control of a large-scale power system subject to consecutive pulse load variations," *IEEE Access*, vol. 5, pp. 26318–26327, 2017.
[12] A. M. Cramer, S. D. Sudhoff, and E. L. Zivi, "Evolutionary algorithms for minimax problems in robust design," *IEEE Trans. Evol. Comput.*, vol. 13, no. 2, pp. 444–453, Apr. 2009.
[13] P. B. Backlund, C. C. Seepersad, and T. M. Kiehne, "All-electric ship energy system design using classifier-guided sampling," *IEEE Trans. Transp. Electrific.*, vol. 1, no. 1, pp. 77–85, Jun. 2015.
[14] N. Doerry, "Zonal ship design," *Nav. Eng. J.*, vol. 118, no. 1, pp. 39–53, Jan. 2006.
[15] D. Kumar and F. Zare, "A comprehensive review of maritime microgrids: System architectures, energy efficiency, power quality, and regulations," *IEEE Access*, vol. 7, pp. 67249–67277, 2019.
[16] A. M. Cramer, S. D. Sudhoff, and E. L. Zivi, "Metric optimization-based design of systems subject to hostile disruptions," *IEEE Trans. Syst., Man, Cybern., A, Syst. Humans*, vol. 41, no. 5, pp. 989–1000, Sep. 2011.
[17] A. Vicenzutti, R. Menis, and G. Sulligoi, "All-electric ship-integrated power systems: Dependable design based on fault tree analysis and dynamic modeling," *IEEE Trans. Transp. Electrific.*, vol. 5, no. 3, pp. 812–827, Sep. 2019.
[18] R. R. Chan, S. D. Sudhoff, Y. Lee, and E. L. Zivi, "A linear programming approach to shipboard electrical system modeling," in *Proc. IEEE Electric Ship Technol. Symp.*, Apr. 2009, pp. 261–269.
[19] A. M. Cramer, H. Chen, and E. L. Zivi, "Shipboard electrical system modeling for early-stage design space exploration," in *Proc. IEEE Electric Ship Technol. Symp. (ESTS)*, Apr. 2013, pp. 128–134.
[20] A. M. Cramer, X. Liu, Y. Zhang, J. D. Stevens, and E. L. Zivi, "Early-stage shipboard power system simulation of operational vignettes for dependability assessment," in *Proc. IEEE Electr. Ship Technol. Symp. (ESTS)*, Jun. 2015, pp. 382–387.
[21] D. Gayme and U. Topcu, "Optimal power flow with large-scale storage integration," *IEEE Trans. Power Syst.*, vol. 28, no. 2, pp. 709–717, May 2013.
[22] K. M. Chandy, S. H. Low, U. Topcu, and H. Xu, "A simple optimal power flow model with energy storage," in *Proc. 49th IEEE Conf. Decis. Control (CDC)*, Dec. 2010, pp. 1051–1057.
[23] D. F. Opila, J. D. Stevens, and A. M. Cramer, "The role of future information in control system design for shipboard power systems," in *Proc. Int. Ship Control Syst. Symp. (iSCSS)*, Glasgow, U.K., Oct. 2018.
[24] R. D. Zimmerman, C. E. Murillo-Sanchez, and R. J. Thomas, "MATPOWER: Steady-state operations, planning, and analysis tools for power systems research and education," *IEEE Trans. Power Syst.*, vol. 26, no. 1, pp. 12–19, Feb. 2011.
[25] E. Oh, D. F. Opila, J. Stevens, E. Zivi, and A. Cramer, "Early stage design evaluation of shipboard power systems using multi-period power flow," in *Proc. IEEE Electric Ship Technol. Symp. (ESTS)*, Aug. 2017, pp. 225–231.
[26] C. E. Murillo-Sanchez, R. D. Zimmerman, C. Lindsay Anderson, and R. J. Thomas, "Secure planning and operations of systems with stochastic sources, energy storage, and active demand," *IEEE Trans. Smart Grid*, vol. 4, no. 4, pp. 2220–2229, Dec. 2013.
[27] A. Anvari-Moghaddam, T. Dragicevic, L. Meng, B. Sun, and J. M. Guerrero, "Optimal planning and operation management of a ship electrical power system with energy storage system," in *Proc. 42nd Annu. Conf. IEEE Ind. Electron. Soc. (IECON)*, Oct. 2016, pp. 2095–2099.
[28] L. W. Y. Chua, T. Tjahjowidodo, G. G. L. Seet, and R. Chan, "Implementation of optimization-based power management for all-electric hybrid vessels," *IEEE Access*, vol. 6, pp. 74339–74354, 2018.
[29] S. Bose, S. Pal, B. Natarajan, C. M. Scoglio, S. Das, and N. N. Schulz, "Analysis of optimal reconfiguration of shipboard power systems," *IEEE Trans. Power Syst.*, vol. 27, no. 1, pp. 189–197, Feb. 2012.
[30] M. Kraning, Y. Wang, E. Akuiyibo, and S. Boyd, "Operation and configuration of a storage portfolio via convex optimization," *IFAC Proc. Volumes*, vol. 44, no. 1, pp. 10487–10492, Jan. 2011.
[31] F. J. R. Verbruggen, V. Rangarajan, and T. Hofman, "Powertrain design optimization for a battery electric heavy-duty truck," in *Proc. Amer. Control Conf. (ACC)*, Philadelphia, PA, USA, Jul. 2019, pp. 1488–1493.
[32] K. Han, Y. Wang, D. Filev, E. Dai, I. Kolmanovsky, and A. Girard, "Optimized design of multi-speed transmissions for battery electric vehicles," in *Proc. Amer. Control Conf. (ACC)*, Philadelphia, PA, USA, Jul. 2019, pp. 816–821.
[33] S. Bose, D. F. Gayme, U. Topcu, and K. M. Chandy, "Optimal placement of energy storage in the grid," in *Proc. IEEE 51st IEEE Conf. Decis. Control (CDC)*, Dec. 2012, pp. 5605–5612.
[34] J. D. Stevens, D. F. Opila, A. M. Cramer, and E. L. Zivi, "Operational vignette-based electric warship load demand," in *Proc. IEEE Electric Ship Technol. Symp. (ESTS)*, Jun. 2015, pp. 213–218.
[35] F. Li, Y. Chen, R. Xie, C. Shen, L. Zhang, and B. Qin, "Optimal operation planning for orchestrating multiple pulsed loads with transient stability constraints in isolated power systems," *IEEE Access*, vol. 6, pp. 18685–18693, 2018.
[36] W. Du, G. Yang, C. Pan, and P. Xi, "A heterogeneous multi-agent system model with navigational feedback for load demand management of a zonal medium voltage DC shipboard power system," *IEEE Access*, vol. 7, pp. 148073–148083, 2019.
[37] G. L. Sinsley, D. F. Opila, and J. Stevens, "Dynamically coupled process control and power management for shipboard power and energy system applications," in *Proc. IEEE Electric Ship Technol. Symp. (ESTS)*, Aug. 2019, pp. 619–626.
[38] N. Alguacil and A. J. Conejo, "Multiperiod optimal power flow using benders decomposition," *IEEE Trans. Power Syst.*, vol. 15, no. 1, pp. 196–201, Feb. 2000.
[39] D. Kourounis, A. Fuchs, and O. Schenk, "Toward the next generation of multiperiod optimal power flow solvers," *IEEE Trans. Power Syst.*, vol. 33, no. 4, pp. 4005–4014, Jul. 2018.
[40] Z. Wang, J. Zhong, D. Chen, Y. Lu, and K. Men, "A multi-period optimal power flow model including battery energy storage," in *Proc. IEEE Power Energy Soc. Gen. Meeting*, Jul. 2013, pp. 1–5.
[41] A. Gopalakrishnan, A. U. Raghunathan, D. Nikovski, and L. T. Biegler, "Global optimization of multi-period optimal power flow," in *Proc. Amer. Control Conf.*, Jun. 2013, pp. 1157–1164.
[42] H. Oh, "Optimal planning to include storage devices in power systems," *IEEE Trans. Power Syst.*, vol. 26, no. 3, pp. 1118–1128, Aug. 2011.
[43] A. J. Wood, B. F. Wollenberg, and G. B. Sheblé *Power Generation, Operation, and Control*. Hoboken, NJ, USA: Wiley, 2013.
[44] K. L. Butler, N. D. R. Sarma, and V. Ragendra Prasad, "Network reconfiguration for service restoration in shipboard power distribution systems," *IEEE Trans. Power Syst.*, vol. 16, no. 4, pp. 653–661, Nov. 2001.
[45] G. Poyrazoglu and H. Oh, "Optimal topology control with physical power flow constraints and N-1 contingency criterion," *IEEE Trans. Power Syst.*, vol. 30, no. 6, pp. 3063–3071, Nov. 2015.
[46] J. S. Chalfant and C. Chryssostomidis, "Analysis of various all-electric-ship electrical distribution system topologies," in *Proc. IEEE Electric Ship Technol. Symp.*, Apr. 2011, pp. 72–77.
[47] J. D. Stevens, D. F. Opila, E. S. Oh, and E. L. Zivi, "All-electric warship load demand model for power and energy system analysis using exogenously initiated threats," in *Proc. IEEE Electric Ship Technol. Symp. (ESTS)*, Aug. 2017, pp. 486–492.

GREGORY L. SINSLEY (Member, IEEE) received the B.S. degree in electrical engineering from the Grove City College, Grove City, PA, USA, in 2005, and the Ph.D. degree in electrical engineering from Pennsylvania State University, University Park, PA, USA, in 2012. He was an Electrical Engineer with Applied Technology, Inc., from 2012 to 2016, and an Electronics Engineer with the United States Naval Research Laboratory, from 2016 to 2018. He has been an Assistant Research Professor with the Electrical and Computer Engineering Department, United States Naval Academy, Annapolis, MD, USA, since 2018. His research interests include optimization and control of power systems, multisensor data fusion, and anomaly detection in cyber-physical systems.

DANIEL F. OPILA (Member, IEEE) received the B.S. and M.S. degrees from the Massachusetts Institute of Technology, Cambridge, MA, USA, in 2002 and 2003, respectively, and the Ph.D. degree from the University of Michigan, Ann Arbor, MI, USA, in 2010. He is currently an Associate Professor of electrical and computer engineering with the United States Naval Academy, Annapolis, MD, USA. He has previously worked in various engineering positions at GE Power Conversion, Ford Motor Company, Orbital Sciences Corporation, and Bose Corporation. His research interests include optimal control of energy systems, hybrid vehicles, naval power systems, power converters, and renewables. He was a recipient of the 2014 IEEE TRANSACTIONS ON CONTROL SYSTEMS TECHNOLOGY Outstanding Paper Award.

EUN S. OH (Member, IEEE) received the B.S. degree from the Swarthmore College, in 1996, the M.S. degree from Johns Hopkins University, in 1999, and the M.S. and Ph.D. degrees from the University of Virginia, in 2013 and 2015, respectively. He is currently a Science Advisor of the Office of Under Secretary of Defense Research and Engineering, Quantum Science Office, Pentagon. He has previously served as the Science Advisor of the Defense Threat Reduction Agency Research and Development–Threat Technologies Directorate. He also worked as an Assistant Research Professor with the United States Naval Academy, a Physicist at the United States Naval Research Laboratory, and a Scientist at the National Aeronautics and Space Administration Goddard Space Flight Center. His research interests include astrophysics to quantum physics, including optimization relating physics to engineering phenomena.

JOHN D. STEVENS (Member, IEEE) received the B.S. degree from the United States Naval Academy, Annapolis, MD, in 1993, and the Ph.D. degree in electrical engineering from the Naval Postgraduate School, Monterey, CA, in 2007. He is currently an Assistant Professor with the Electrical and Computer Engineering Department, United States Naval Academy. His research interests include naval power systems, electric machinery, and pulse load applications. As a Naval Officer for over 27 years, he has served on various naval warships and numerous navy research and development programs that advance naval power system capabilities.